buildings

MDPI

Article

Numerical Study Regarding the Seismic Response of a Moment-Resisting (MR) Reinforced Concrete (RC) Frame Structure with Reduced Cross-Sections of the RC Slabs

Ion Socol [1], Petru Mihai [2], Tudor-Cristian Petrescu [2,*], Florin Nedeff [3,*], Valentin Nedeff [4], Maricel Agop [5,6] and Bogdan-Ionel Luca [1]

[1] Doctoral School of Faculty of Civil Engineering and Building Services, "Gheorghe Asachi" Technical University of Iasi, 43 Dimitrie Mangeron Blvd., 700050 Iasi, Romania
[2] Department of Concrete, Materials, Technology and Management, Faculty of Civil Engineering and Building Services, "Gheorghe Asachi" Technical University of Iasi, 43 Dimitrie Mangeron Blvd., 700050 Iasi, Romania
[3] Department of Environmental Engineering and Mechanical Engineering, Faculty of Engineering, "Vasile Alecsandri" University of Bacău, 600115 Bacău, Romania
[4] Department of Industrial Systems Engineering and Management, Faculty of Engineering, "Vasile Alecsandri" University of Bacău, 600115 Bacău, Romania
[5] Department of Physics, Faculty of Machine Manufacturing and Industrial Management, "Gheorghe Asachi" Technical University of Iasi, 700050 Iasi, Romania
[6] Academy of Romanian Scientists, 050094 Bucharest, Romania
* Correspondence: tudor.petrescu@tuiasi.ro (T.-C.P.); florin_nedeff@yahoo.com (F.N.)

Abstract: In the first part of the current study, the effectiveness of the transversal cross-section reduction method for RC beams in marginal areas (by means of mechanical drilling) was validated. The said method "encourages" the formation of plastic hinges at the beam ends and, at the same time, allows for taking into account the bending stiffness of RC slabs, which is exerted upon the RC beams. In these conditions, the second part of the current research study (i.e., the current manuscript) highlights the real mode of reducing the lateral stiffness of the slabs upon the RC beams. These elements form a common body, together with the beam–column frame node. The same method as in the first part of the study—"weakening" the plates in the corner area through vertical drilling, without affecting the integrity of the reinforcing elements—was used. The analytical MR RC frame model, studied by means of the comparative method, highlights the efficiency of the transversal cross-section reduction method for RC slabs. Basically, the directing of the plastic deformations from the weakened slab areas towards the marginal areas of the reinforced concrete beams takes place. The beams rotate as far as the weakened slab areas allow its plastic deformation, thus being possible to observe the partial conservation effect of the beam–column frame joint. Furthermore, for the analytical model with the maximum number of vertical holes in the corner areas of the concrete plate, minimal plastic deformations are recorded for the marginal areas of the concrete columns. A partial conservation of the formation mechanism of the "beam-slab-frame node" common rigid block is also noted. Consequently, the dissipation of the seismic energy is made in a partially controlled and directed manner, in the "desired" areas, according to the "Strong Columns—Weak Beams" (SCWB) ductile mechanism of the lateral behavior to seismic actions for reinforced concrete frame structures. The mechanism is specified in current design norms for RC frame systems. The effectiveness of the method for reducing the transversal section of the RC plates in the corner areas by means of transversal drilling is highlighted and validated from the perspective of the local and global ductile seismic response of reinforced concrete frame structures. A significant reduction in the bending stiffness of the slabs upon the beams and a real development of the plastic hinges in the marginal areas of the beams (together with partial implications and plastic deformations) were observed.

Keywords: FEM analysis; pushover; RC slabs; frame structure; vertical holes; plastic zones

check for updates

Citation: Socol, I.; Mihai, P.; Petrescu, T.-C.; Nedeff, F.; Nedeff, V.; Agop, M.; Luca, B.-I. Numerical Study Regarding the Seismic Response of a Moment-Resisting (MR) Reinforced Concrete (RC) Frame Structure with Reduced Cross-Sections of the RC Slabs. *Buildings* **2022**, *12*, 1525. https://doi.org/10.3390/buildings12101525

Academic Editors: Radu Vacareanu and Florin Pavel

Received: 5 August 2022
Accepted: 19 September 2022
Published: 23 September 2022

1. Introduction

The numerical analyses [1–9] pertaining to experimental studies [1,2,10] and to the effects of on-site earthquakes upon seismic-resistant reinforced concrete frame structures [11–16] prove the incapacity of such a structural system to develop a ductile seismic energy dissipative mechanism.

The marginal areas of the reinforced concrete columns [1–10] and the beam–column frame nodes [2,17] deform intensively and are the main elements with a plastic behavior for these types of structural systems [18].

Furthermore, it is possible to highlight the development of the "beam-column-frame node" common rigid block when a seismic event occurs. The rigid block is conducive to the concentration of plastic hinges in the marginal areas of the reinforced concrete columns and in the beam–column frame joints [19–27].

In these circumstances, several practical solutions are proposed regarding the improvement of the seismic response of MR RC frame systems. One such solution for the reduction of the transversal section of the reinforced concrete beams is by means of drilling them in critical areas in a transversal direction. The solution was presented in the first part of the current research study, carried out by Socol et al. [28].

Additionally, in this first part [28] of the current analytical study, the research topic was aligned with the existing notions in current seismic design norms, resulting in the emergence of a substantial literature review section.

Therefore, in the second part of the current analytical study, it is proposed to reduce the transversal section of the RC slabs through the same method of drilling in a transversal direction. This is carried out in the corner areas for the K_7 (representative) analytical MR RC frame model [9,28], (see Figure 1a).

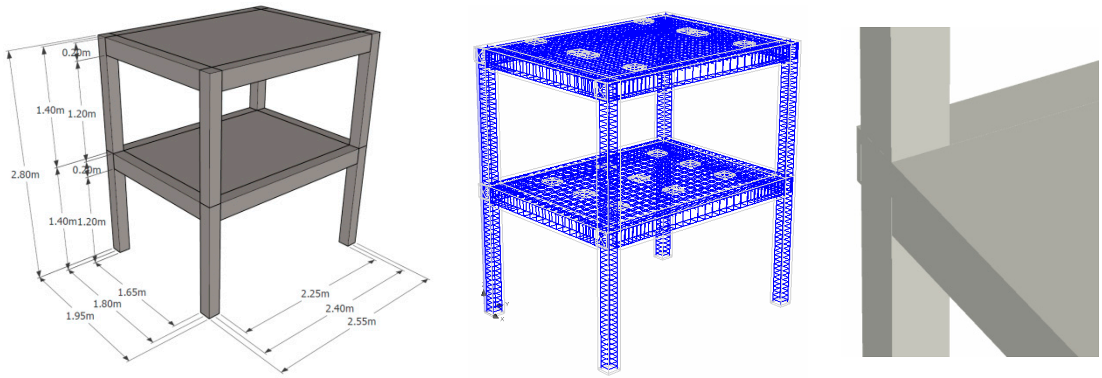

(**a**) (**b**) (**c**)

Figure 1. Graphical representation of the K_7 MR RC frame model (reduced to $\frac{1}{2}$ scale) (Reprinted from Ref. [28]): (**a**) "Global tridimensional representation of the structural system" [8,9,28]; (**b**) "Steel reinforcement carcase in MR RC frame model" [8,9,28]; (**c**) "Local representation of the reinforced concrete beam-column frame joint at the level of the slab over the ground story" [28].

The main contribution of this paper is the improvement of the seismic response of MR RC frame systems. This subject is considered to be of importance, as it is possible to observe the reduction of the in-plane rigidization effect of the beams upon the concrete slab. Moreover, it allows the possibility to analytically validate the proposed solution, such that the dissipation of the seismic energy will occur through the development of the "Strong Columns—Weak Beams" (SCWB) mechanism [29,30].

2. Methodology

The comparative research method of the current analytical study contains the following distinct steps:

- The research and the presentation of the issues regarding the non-ductile mechanism developed by reinforced concrete frame structures which undergo dynamic loading;
- The registering and the presentation of the local seismic energy dissipation mechanisms, which appear in the lateral elements of the said type of structural system, and the highlighting of the rigidization effect of the RC beams upon the RC slab;
- The development and the presentation of a possible solution for the concentration of plastic deformations in the marginal areas of the beams and the corner areas of the slabs, by means of reducing the transversal section of the slabs;
- The analytical (numerical) validation of the proposed solution.

3. Pushover Analysis of the GF + 1F Moment-Resisting (MR) Reinforced Concrete (RC) Frame Model

3.1. General Aspects

Within the scope of the current analytical study, numerical analyses were performed with the ATENA computer program [31–40]. The representative analytical model is considered to be the K_7 MR RC frame system specified by Sococol et al. [8,9,28] (also see Figure 1a and Table 1). All subsequently generated analytical models found in the current study have, as a source, the model K_7.

Table 1. Principal characteristic parameters considered in numerical analyses of the **M**oment-**R**esisting (MR) **R**einforced **C**oncrete (RC) frame models.

NSC	CSC	LSRT	TSRT	LSR RC C [CS:15 × 15 cm]	LSR RC LB [CS:15 × 20 cm]	LSR RC TB [CS:15 × 20 cm]	TSR RC C	TSR RC LB and TB	R RC S [h_s = 7 cm]	GR
K_7	C20/25	Bst 500S	Bst 500M	4ϕ14	4ϕ8	4ϕ8	1ϕ4/1 CS	1ϕ4/1 CS	ϕ6	Figure 1b
K_7_S_2										Figure 2(a2)
K_7_S_1										Figure 2(b2)
K_7_S_B_1										Figure 2(c2)

Note: NSC—**N**umerical **S**imulation **C**ode; CSC—**C**oncrete **S**trength **C**lass; LSRT—**L**ongitudinal **S**teel **R**einforcement **T**ype; TSRT—**T**ransverse **S**teel **R**einforcement **T**ype; LSR—**L**ongitudinal **S**teel **R**einforcement; RC—**R**einforced **C**oncrete; C—**C**olumns; CS—**Cross-section**; LB—**L**ongitudinal **B**eams; TB—**T**ransverse **B**eams; TSR—**T**ransverse **S**teel **R**einforcement; R—**R**einforcement; S—**S**labs; h_s–slabs' thickness; GR—**G**raphical **R**epresentation. (Additional specifications: LSR RC C, TSR RC C, LSR RC LB, LSR RC TB, TSR RC LB, TSR RC TB, and R RC S can be consulted in the research study carried out by Sococol et al. [28]).

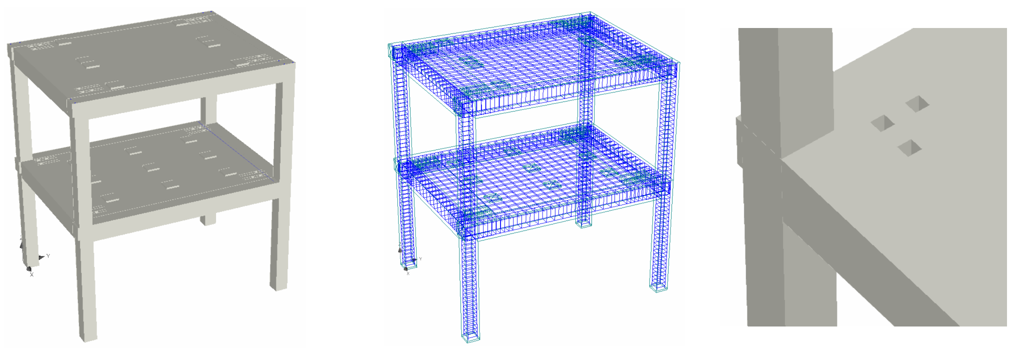

(a1) **(a2)** **(a3)**

(a)

Figure 2. *Cont.*

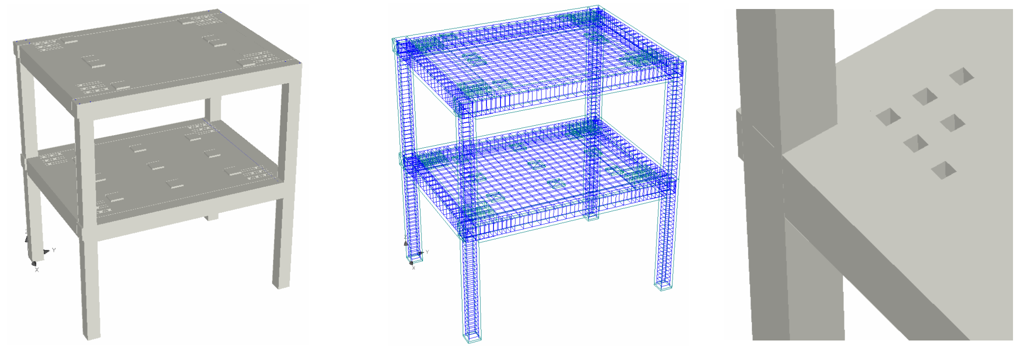

(**b1**) (**b2**) (**b3**)

(**b**)

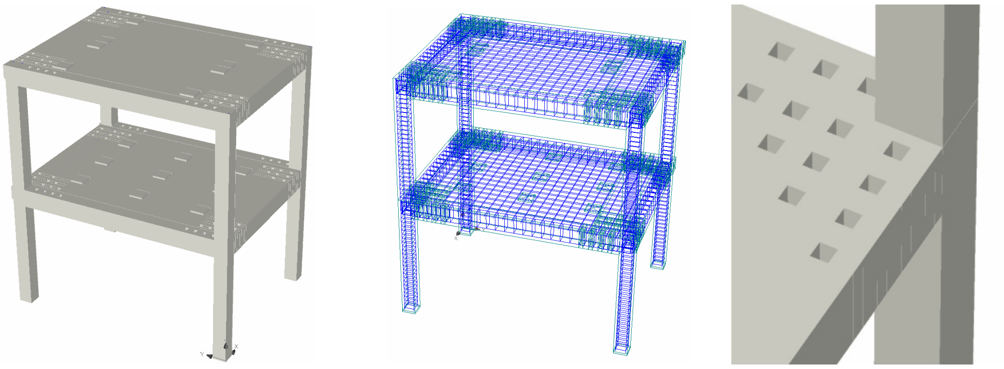

(**c1**) (**c2**) (**c3**)

(**c**)

Figure 2. Graphical representation of the analytical MR RC frame models: (**a**) K_7_S_2; (**b**) K_7_S_1; (**c**) K_7_S_B_1: (**a1**), (**b1**), and (**c1**), "Global tridimensional representation of the structural system" [8,9,28]; (**a2**), (**b2**), and (**c2**), "Steel reinforcement carcase in MR RC frame model" [8,9,28]; (**a3**), (**b3**), and (**c3**), "Local representation of the reinforced concrete beam-column frame joint at the level of the slab over the ground story" [28].

In these circumstances, each analytical model contains reinforced concrete slabs with a reduced transversal section in the corner areas by means of employing the process of transversal mechanical drilling (see Figure 1).

Each structure of the reinforced concrete frame type was loaded with equivalent static forces in the horizontal direction, parallel to the long side of the lateral system (see Figure 3), according to the recommendations specified by P100-1 [29] and in EC 8 [30].

Thus, the "F-D" (Force–Displacement) capacity curves and the specific maximum deformation curves were obtained, being numerically described in Section 3. Furthermore, the deformation mode for each analytical model was observed via graphical visualization and studying of the crack pattern for each lateral loading step. Within the current study, the frame models are graphically represented only for the final lateral loading step, in order to simplify and reduce the volume of information to be visualized.

The numerical analyses display and validate the developing process of the "beam-plate-frame node" common rigid block [5–9,41–43] for both the unaltered analytical model, as well as for the modified one (by means of mechanical drilling in the plates, in the corner areas). Consequently, the rigidization effect of the reinforced concrete beams, produced by the plates, will be significantly reduced.

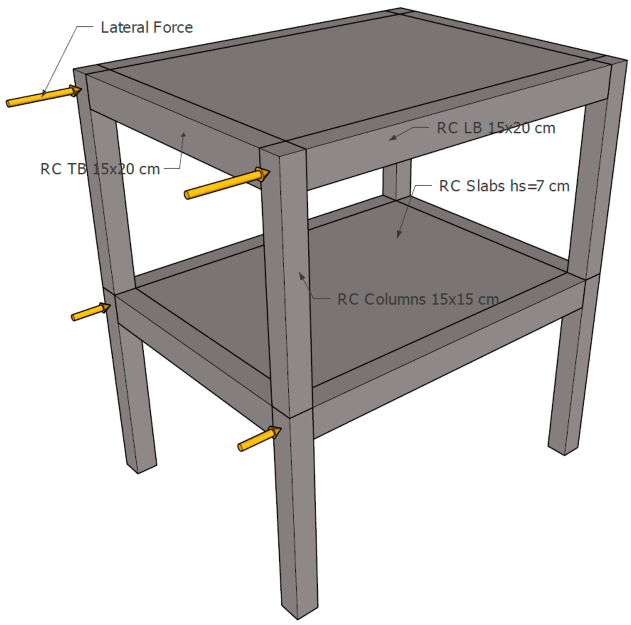

Figure 3. "Lateral loading consideration for pushover analysis of the K_7 MR RC frame system" [28] (Reprinted from Ref. [28]).

3.2. Input Data Considered in Research Study

The reinforced concrete frame type models were reduced to a $\frac{1}{2}$ scale according to the similitude criteria specified by El-Attar et al. [44], Harris and Sabnis [45], Moncarz and Krawinkler [46], as well as other scientific literature sources [47–52]. These models were horizontally loaded (on the long direction of the structural system) with static equivalent forces obtained in the linear elastic calculus stage, in accordance with Figure 3.

The disposition of reinforcement for the lateral structure, for each RC frame model, was represented in the research study carried out by Sococol et al. [28]. Moreover, the "meshed model" [32,53,54], for which the "stress-strain relations for concrete" [55–60] and "stress-strain laws for steel reinforcement" [55,61–64], were respected. These can also be found in Sococol et al. [28].

The input data required for the numerical simulations are presented in Tables 1 and 2.

In Table 2, the main aspects regarding the method of reducing the cross-section of the reinforced concrete slabs (by means of transversal drilling of the corner areas—with the purpose of reducing the influence of the bending stiffness of the slabs upon the beams), such that the plastic hinges will develop in the marginal areas of the RC beams, are specified.

In these circumstances, "within the scope of the numerical simulations, the drilled holes were considered to have a square shape, both in order to simplify the generation of the meshing for the structural elements and to avoid the occurrence of several analytical problems regarding the interaction between concrete and welded wire nets" [7,28,53,54], etc.

The number of vertically drilled holes in the reinforced concrete slabs was established according to the following criteria:

- They should not compromise the structural integrity of the welded wire nets, therefore the holes are placed in-between the wires;
- They should be emplaced at a minimum distance from the reinforced concrete frame nodes and columns. Said distance was established taking into account the first gaps in the welded wire nets, which could be found outside of the beam–column frame node;
- The drilling surface has a triangular shape and the length of the two sides parallel to the RC beams is equal to "the length of the plastic hinge from the RC beams, computed according to P100-1 [29] norm for each type of beam (longitudinal and transversal)" [28].

Table 2. Main aspects regarding the cross-section reducing method of the RC slabs through the vertical drilling (mechanical) process in the corner areas for analytical MR RC frame models.

NSC	RC Drilled Element Type in the Potentially Plastic Zone	Holes' Type Depends on the Geometric Shape (Form)	Variable (V)/Constant (C) Size Holes	Number of Holes	Number of Rows of Holes	Constant (C)/Variable (V) Distance between Holes	Constant (C)/Variable (V) Distance between Rows of Holes	Minimum (Min)/Maximum (Max) Distance between Holes and RC B-C Joint/RC Column	Rows of Vertical Holes Positioning (Zig-Zag, Parallel, etc.)	Transverse Reinforcement Mode of the RC Columns	GR
K_7	-	-	-	-	-	-	-	-	-	1ϕ4/1 CS	Figure 1a,c
K_7_S_2	slab	square holes	C	3	1	C	-	Min.	-	1ϕ4/1 CS	Figure 2 (a1),(a3)
K_7_S_1	slab	square holes	C	6	2	C	C	Min.	parallel	1ϕ4/1 CS	Figure 2 (b1),(b3)
K_7_S_B_1	beam and slab	square holes	C	4 for LB 3 for TB 6 for RC slab	1 for LB 1 for TB 2 for RC slab	C	- - C	Min.	- - parallel	1ϕ4/1 CS	Figure 2 (c1),(c3)

Note: Vertical holes were positioned between the RC slabs' (steel) reinforcement bars, without affecting the structural integrity of these structural elements (see Sococol et al. [28]). NSC—**N**umerical **S**imulation **C**ode; RC—**R**einforced **C**oncrete; LB—**L**ongitudinal **B**eams; TB—**T**ransverse **B**eams; CS—**Cross-section**; GR—**G**raphical **R**epresentation.

"It is mentioned the fact that it was avoided to go into too much detail regarding the influence of the geometric shape of the holes, the variability of the dimensions of the holes, the constant/variable distance between the holes, the constant/variable distance between the rows with holes, the zig-zag/parallel positioning of the rows with holes etc." [28], in order to simplify the numerical calculus stages, as well as the number of numerical analyses to be performed.

In these conditions, Figures 1 and 2 tridimensionally depict the RC frame models K_7, K_7_S_2, K_7_S_1 and K_7_S_B_1 together with their corresponding reinforcement skeleton and the beam–column frame node from the level of the plate over the ground story, in order to be able to visualize the transversal drilling of the slabs.

4. Analytical Results and Complementary Comments

4.1. Analytical Results

The non-linear static analyses (SPO) made for the analytical MR RC frame models specified in Tables 1 and 2 and Figures 1 and 2 show not only the numerical results for the "ultimate lateral forces (F_u), ultimate lateral displacements (d_u), lateral forces corresponding to the yielding of the equivalent SDOF system (F^*_y), horizontal displacements at the top of the structure corresponding to the yielding of the equivalent SDOF system (d^*_y), total specific strain Eps zz, principal fracture strain" [5–9,28], (see Table 3) but also the cracking pattern corresponding to each of the studied analytical models in the final horizontal loading step.

Table 3. Analytical results in lateral forces, horizontal displacements, and specific deformations for K_7, K_7_S_2, K_7_S_1, and K_7_S_B_1 laterally loaded structural MR RC frame models with equivalent static forces.

NSC	F_u [kN]	d_u [m]	F^*_y [kN]	d^*_y [m]	SPO CB	TSE (CF)	TSE (TF)	GR TSE (CF/TF)	PFSM	GR PFSM
K_7	41.575	0.03288	40	0.0187	Figure 4a	0.002789	0.006118	Figure 5 (a5),(a6)	0.0413	Figure 5 (a1)–(a4)
K_7_S_2	39.49625	0.02785	37.8	0.0169	Figure 4b	0.002267	0.003946	Figure 5 (b5),(b6)	0.02573	Figure 5 (b1)–(b4)
K_7_S_1	39.49625	0.028	38.2	0.0173	Figure 4c	0.002295	0.003982	Figure 5 (c5),(c6)	0.01905	Figure 5 (c1)–(c4)
K_7_S_B_1	41.575	0.03179	40.4	0.0188	Figure 4d	0.002693	0.00576	Figure 5 (d5),(d6)	0.02913	Figure 5 (d1)–(d4)

Note: NSC—**N**umerical **S**imulation **C**ode; F_u—ultimate lateral force corresponding to global system collapse; d_u—ultimate lateral displacement of the structural system; F^*_y—lateral force corresponding to structural yielding of the equivalent SDOF structural system; d^*_y—horizontal peak displacement corresponding to structural yielding of the equivalent SDOF structural system; SPO CB—**S**tatic **P**ush-**O**ver **C**urve **B**ilinearisation; TSE—**T**otal **S**train **E**ps zz; CF—**C**ompressive **F**ailure; TF—**T**ensile **F**ailure; GR—**G**raphical **R**epresentation; PFSM—**P**rincipal **F**racture **S**train **M**ax. Specific deformations values in this table correspond to the final horizontal loading step. SPO curves for all MR RC frame models specified in the current table are graphically represented in Figure 6. **L**ateral **F**orces (LF)—PFSM curves for all MR RC frame models specified in the current table are graphically represented in Figure 7. LF—TSE curves for all MR RC frame models specified in the current table are graphically represented in Figure 8.

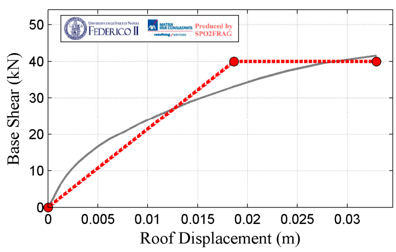

(**a**)

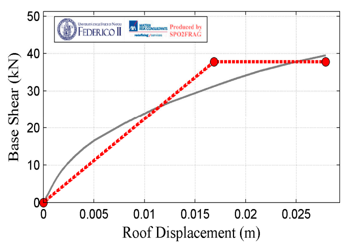

(**b**)

Figure 4. *Cont.*

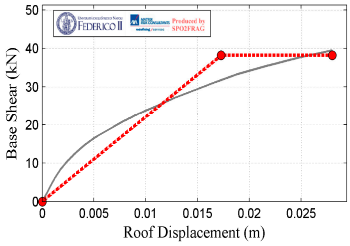

(c)

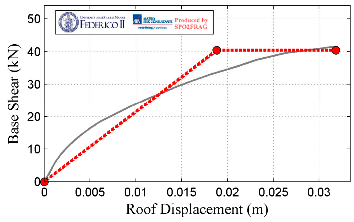

(d)

Figure 4. **S**tatic **P**ush-**O**ver (SPO) curves (gray lines) and bilinearised curves (red lines) [65,66] (bilinearisation process according to elastic—perfectly plastic fit compatible with EC8 indications [30]) for: (**a**) K_7 [8,9,28]; (**b**) K_7_S_2; (**c**) K_7_S_1; (**d**) K_7_S_B_1 MR RC frame models. The implicit values of SPO curves for the final lateral loading step can be studied in Table 3.

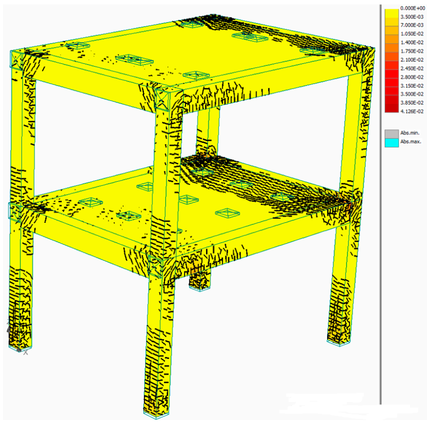

(**a1**)

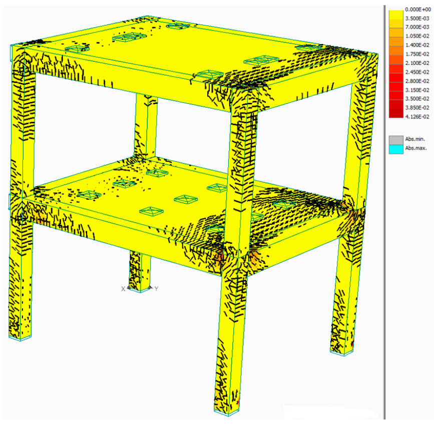

(**a2**)

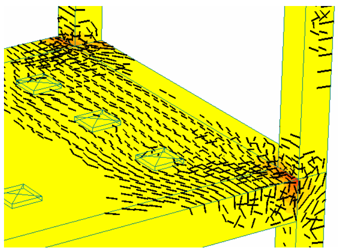

(**a3**)

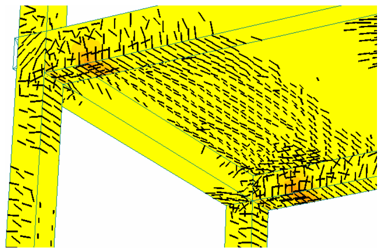

(**a4**)

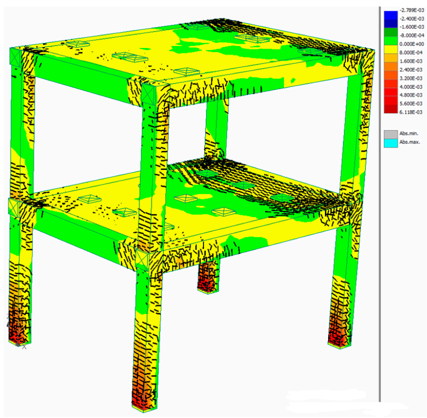

(**a5**)

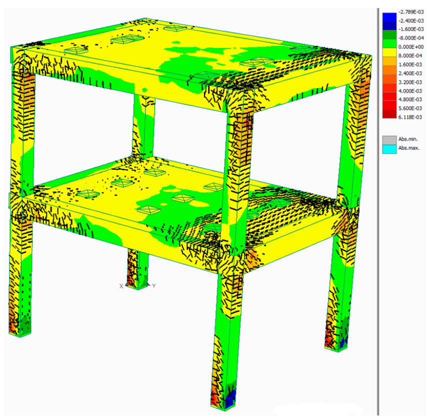

(**a6**)

(**a**)

Figure 5. *Cont.*

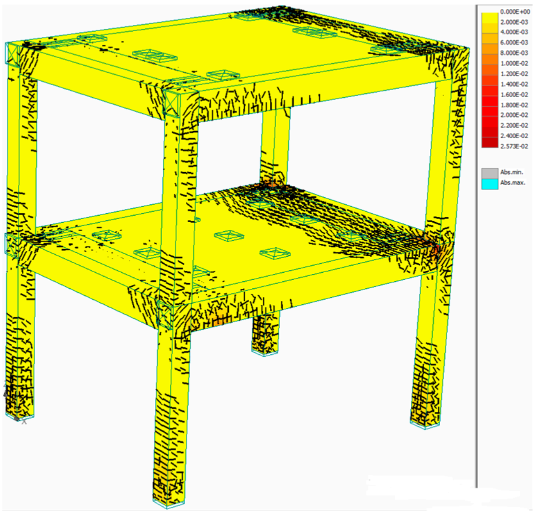

(**b1**)

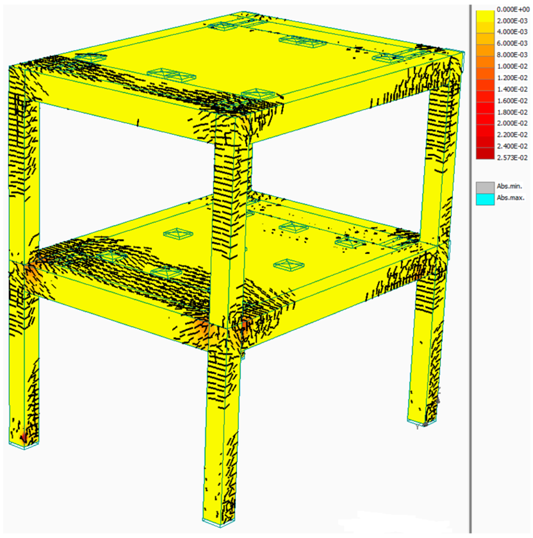

(**b2**)

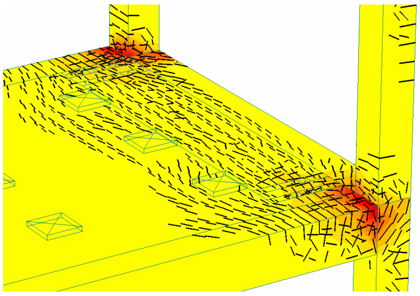

(**b3**)

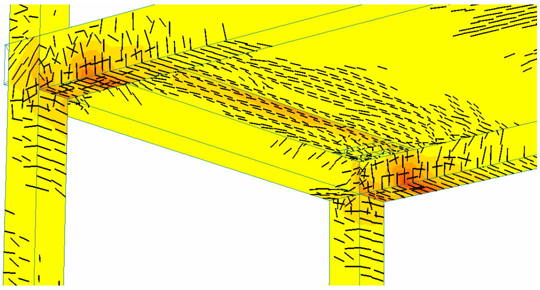

(**b4**)

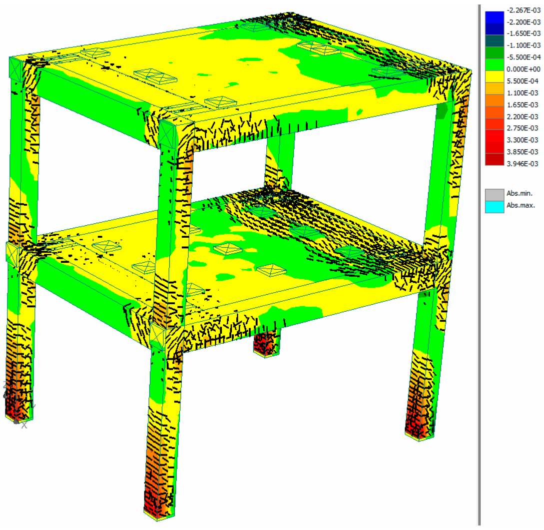

(**b5**)

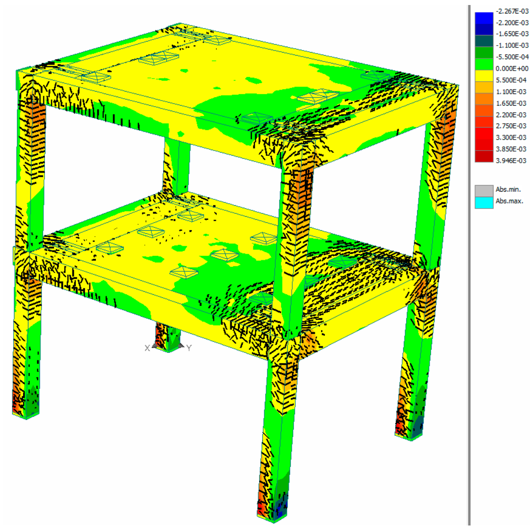

(**b6**)

(**b**)

Figure 5. *Cont.*

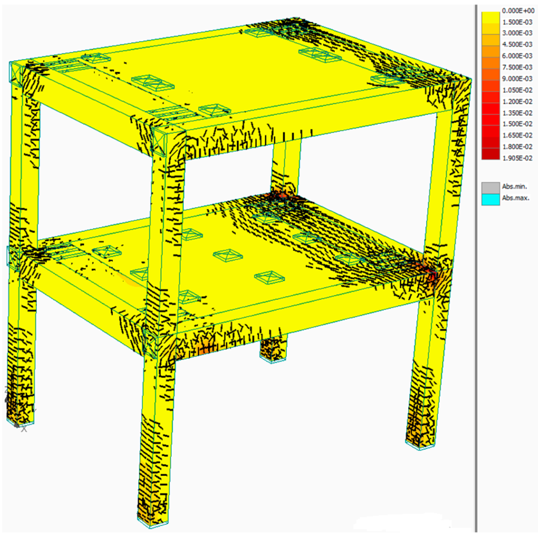

(c1)

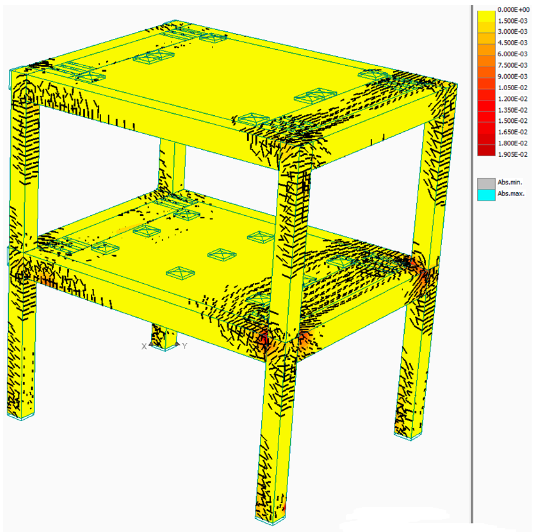

(c2)

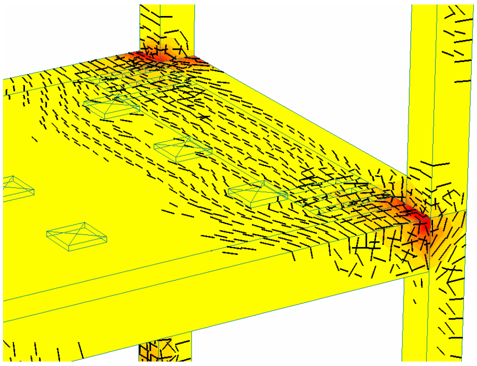

(c3)

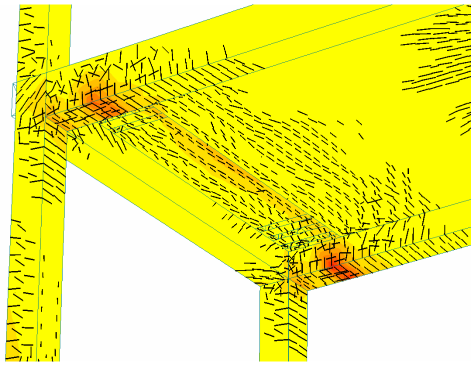

(c4)

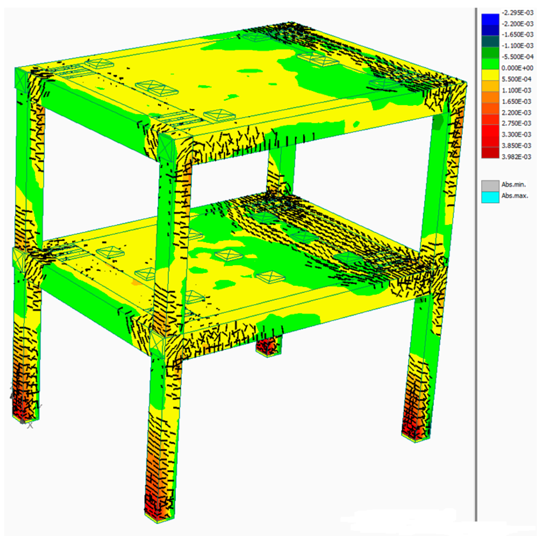

(c5)

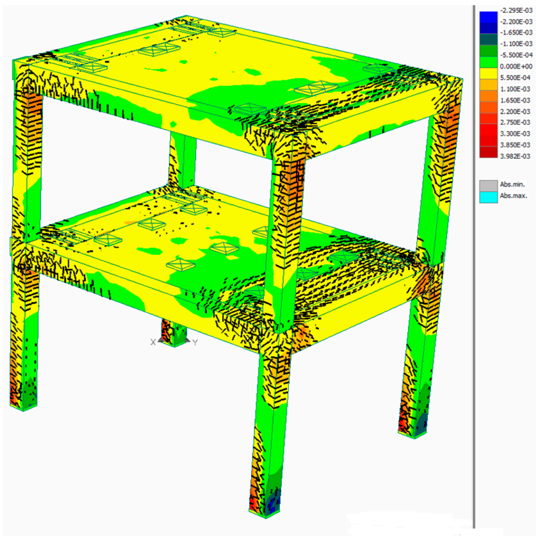

(c6)

(c)

Figure 5. *Cont.*

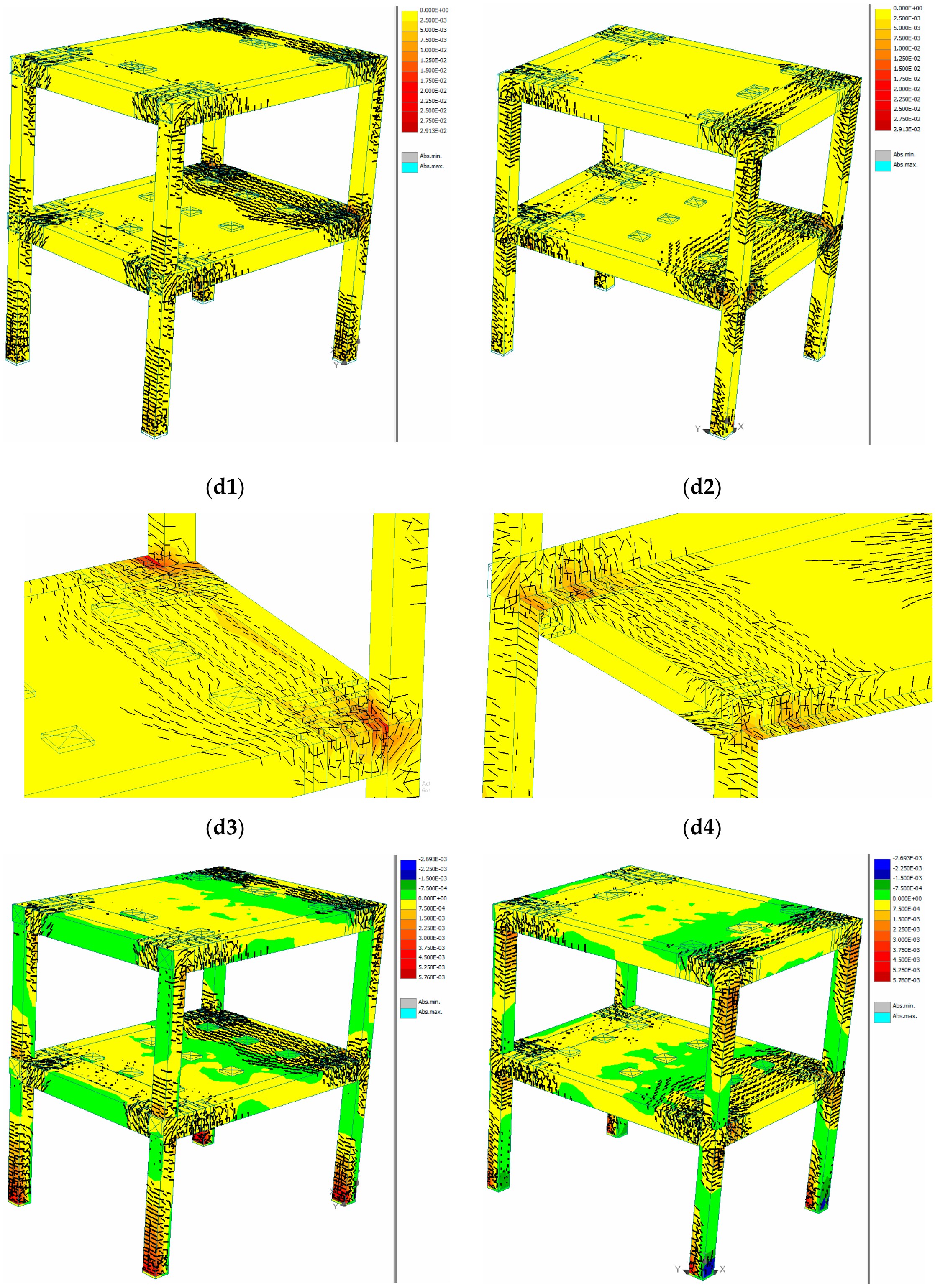

(**d1**) (**d2**)

(**d3**) (**d4**)

(**d5**) (**d6**)

(**d**)

Figure 5. Graphical representation of the deformation and cracking pattern of: (**a**) K_7 [8,9,28] (Reprinted from Ref. [28]); (**b**) K_7_S_2; (**c**) K_7_S_1; (**d**) K_7_S_B_1 **M**oment-**R**esisting (MR) **R**einforced **C**oncrete (RC) frame models for the ultimate lateral loading stage with: (**a1**), (**a2**), (**b1**), (**b2**), (**c1**), (**c2**), (**d1**), and (**d2**) **P**rincipal **F**racture **S**trains **M**ax (PFSM) representations; (**a3**), (**a4**), (**b3**),

(**b4**), (**c3**), (**c4**), (**d3**), and (**d4**) local **P**rincipal **F**racture **S**trains **M**ax (PFSM) representations; (**a5**), (**a6**), (**b5**), (**b6**), (**c5**), (**c6**), (**d5**), and (**d6**) **T**otal **S**trains **E**ps zz (TSE) representations. (Note: In Table 3, the implicit values of PFSM and TSE for the structural element zones with potential plastic deformation (belonging to the (**a**–**d**) MR RC frame analytical models, in their final step of lateral loading) are presented in a tabular form. In Figure 7, the PFSM values expressed as curves are represented for each lateral loading step for the (**a**–**d**) MR RC frame analytical models. In Figure 8, the TSE values expressed as curves are represented for each lateral loading step for the (**a**–**d**) MR RC frame analytical models.

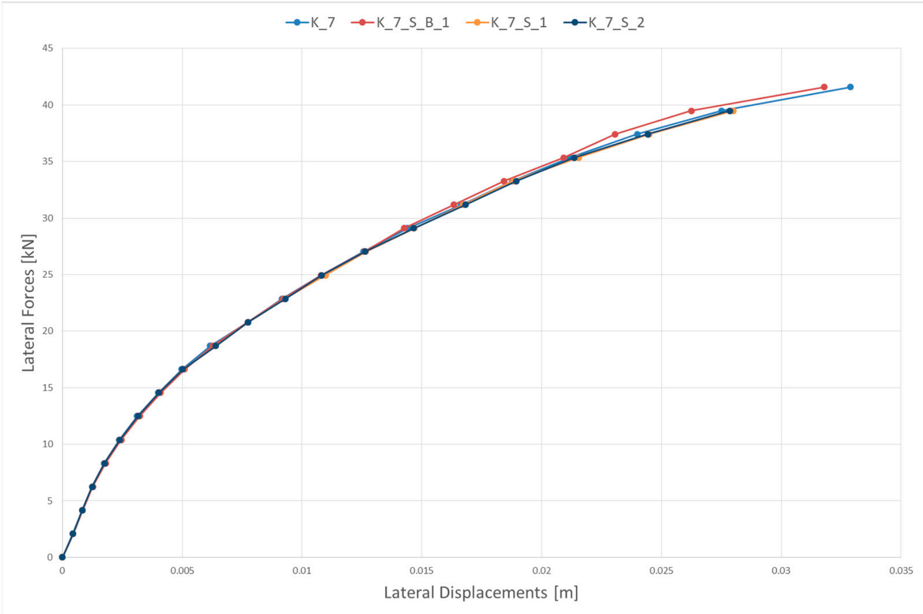

Figure 6. **S**tatic **P**ush-**O**ver (SPO) curves for K_7, K_7_S_B_1, K_7_S_1, and K_7_S_2 **M**oment-**R**esisting (MR) **R**einforced **C**oncrete (RC) frame models.

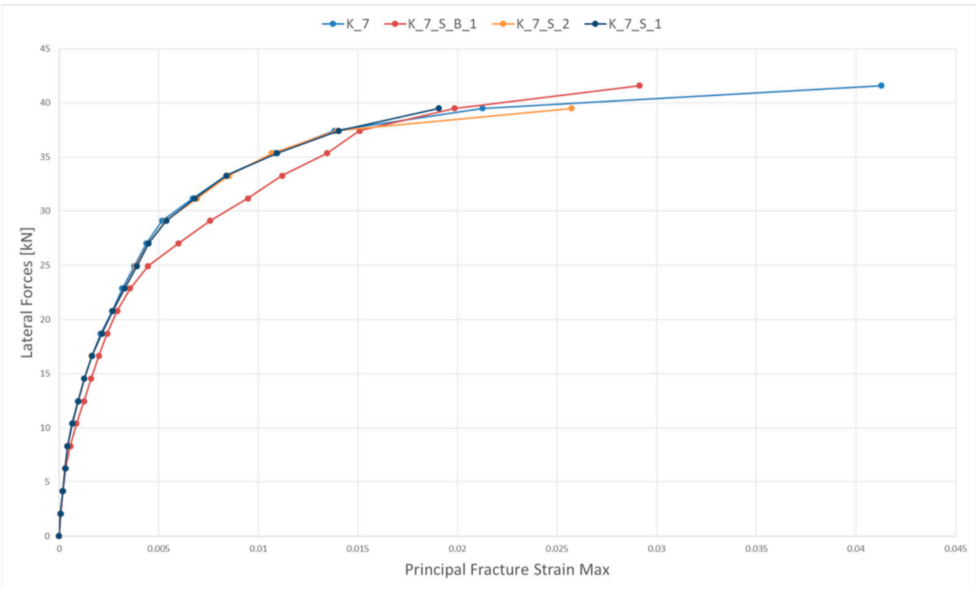

Figure 7. **L**ateral **F**orces (LF)—**P**rincipal **F**racture **S**trains **M**ax (PFSM) curves for K_7, K_7_S_B_1, K_7_S_2, and K_7_S_1 **M**oment-**R**esisting (MR) **R**einforced **C**oncrete (RC) frame models.

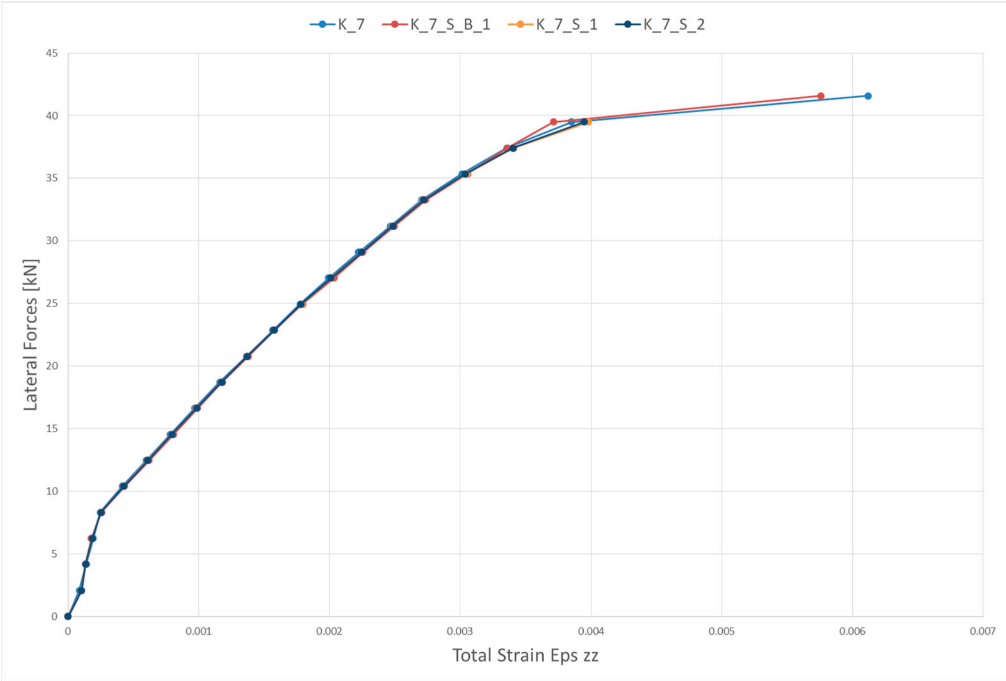

Figure 8. **L**ateral **F**orces (LF)—**T**otal **S**trains **E**ps zz (TSE) curves for K_7, K_7_S_B_1, K_7_S_1, and K_7_S_2 **M**oment-**R**esisting (MR) **R**einforced **C**oncrete (RC) frame models.

The determination of the lateral forces (F^*_y) and lateral displacements (d^*_y) which correspond to the yielding of the equivalent SDOF system, was performed with SPO2FRAG [65,66] computer software, following the bilinearisation of the SPO curves from Figure 6, in accordance with the requirements from Eurocode 8 [30].

The conclusions and the local and global seismic response elements corresponding to the seismic energy dissipation mechanisms are specified in Section 5.

The limit values of the lateral displacements on the top story, for each analytical model, were determined in accordance with:

- P100-1 [29], the Romanian norm;
- EN 1998-1:2004 [30], the European standard associated with the SR EN 1998-1/NA: 2008 [67] national annex;
- Paulay's and Priestley's [68] structural design literature book.

According to P100-1 [29], the Romanian seismic design norm, the admissible value of the relative story displacements is established as follows (see Equation (1)):

$$d_{r,a}^{SLU} = 0.025 \cdot h \tag{1}$$

where

$d_{r,a}^{SLU}$—is the admissible value of the relative story displacement;

h—is the story height.

Therefore, the admissible value for the lateral displacements of the RC frame models, for the top story, is established for h_{top} = 2.8 m.

According to SR EN 1998-1:2004 [30], limiting the relative story displacements for buildings without non-structural elements is performed as follows (see Equation (2)):

$$d_r \vartheta \leq 0.010 \cdot h \tag{2}$$

where

d_r—is the relative story displacement, for the considered story, when performing structural analysis;

h—is the story height;

υ—is the reduction factor, which takes into account the smallest return period of the seismic action associated with requirements for limiting degradations.

Therefore, the limit value for the lateral displacements of the RC frame models, for the top story, is established for h_{top} = 2.8 m.

The value of the reduction factor "*υ*" is established in accordance with SR EN 1998-1/NA: 2008 [67] for the building importance class III of the type of construction analyzed in the current analytical study. As such, *υ* = 0.4.

According to Paulay and Priestley [68], the admissible story drift for a multiple-story structure is 2.5. Story drift is computed as a function of ductility (see Equation (3)):

$$\mu_d = \frac{d_u}{d_y^*} \leq \mu_d^{admissible} = 2.5 \tag{3}$$

where

μ_d—is the ductility of the structural system;

d_u—is the ultimate lateral displacement of the structural system;

$d_y{}^*$—is the horizontal peak displacement corresponding to the structural yielding of the equivalent SDOF structural system;

$\mu_d^{admissible}$—is the admissible ductility of the structural system.

The displacement values "d_u" and "$d_y{}^*$" can be found in Table 3 for each of the studied analytical models.

Consequently, in Table 4, the admissible displacement values for the reinforced concrete frame models are centralized, and the values obtained are in accordance with Equations (1)–(3).

Table 4. Analytical results in terms of admissible lateral displacements and ultimate lateral displacements for K_7, K_7_S_2, K_7_S_1, and K_7_S_B_1 laterally loaded structural MR RC frame models with equivalent static forces.

NSC	$h_{top}{}^{story}$ [m]	d_u [m]	$d_{r,a}{}^{SLU}$ [m]	$h_{top}{}^{story}$ [m]	υ	d_u [m]	d_r [m]	d_u [m]	$d^*{}_y$ [m]	μ_d	$\mu_d{}^{adm}$
	P100-1 [29]			**EN 1998-1:2004 [30]**				**Paulay and Priestley [68]**			
K_7	2.8	0.03288	0.07	2.8	0.4	0.03288	0.07	0.03288	0.0187	1.7582	2.5
K_7_S_2		0.02785				0.02785		0.02785	0.0169	1.6479	
K_7_S_1		0.028				0.028		0.028	0.0173	1.6184	
K_7_S_B_1		0.03179				0.03179		0.03179	0.0188	1.6909	

Note: NSC—**N**umerical **S**imulation **C**ode; $h_{top}{}^{story}$—the total height of the reinforced concrete frame structural models; d_u—ultimate lateral displacement of the structural system; $d_{r,a}{}^{SLU}$—the admissible value of the relative story displacement; υ—the reduction factor, which takes into account the smallest return period of the seismic action associated with requirements for limiting degradations; d_r—the relative story displacement for the considered story when performing structural analysis; $d_y{}^*$—horizontal peak displacement corresponding to structural yielding of the equivalent SDOF structural system; μ_d—the ductility of the structural system; $\mu_d{}^{adm}$—the admissible ductility of the structural system.

Regarding the attainment of the limit values of the lateral displacements, none of the analytical models achieved the admissible threshold specified in the seismic design norms [29,30,67] and in the scientific literature [68]. The obtained result validates the applicability of the method for reducing the transversal section of the concrete slabs in specific areas, with ensured safety conditions regarding the lateral displacements and the structural ductility.

Moreover, a decrease in the overall ductility was observed for the K_7_S_1 and K_7_S_2 analytical models, such that the failure mode of the weakened zones is fragile, localized, and controlled, thus helping in limiting a possible collapse of the structure from the condition of exceeding the admissible lateral displacements.

In addition, the seismic response expressed in forces and lateral displacements at the top of the structure proves that the K_7_S_2 and K_7_S_1 analytical models recorded smaller values than the ones generated for the K_7 model (see Table 3, Figure 6). This effect also makes sense from the perspective of specific maximum rupture strains (see Figures 7 and 8). Their grouping takes place in the weakened slab sectors (corner areas), with favorable effects on the bending mode of the reinforced concrete beams in both principal directions (see Figure 5b,c).

Thus, the K_7_S_2 and K_7_S_1 analytical models consistently help to improve the ductile seismic response, promoting, for the analytical case with a larger number of vertical holes in the corner areas of the slab (the K_7_S_1 model), the development of the grouping process for plastic hinges in the marginal areas of the reinforced concrete beams—together with the partial conservation effect of the beam–column frame joint (Figure 5c).

Nonetheless, the final failure process has a complex nature, occurring in the beams, slabs [69–71], and beam–column frame nodes (see Figure 5b,c), with implications in the non-linear behavior domain in the marginal areas of the columns. This is very different from the idealized form specified in current seismic design norms for structures with plastic hinges in the marginal beam areas and from the "Strong Columns—Weak Beams" (SCWB) seismic energy dissipation mechanism [29,30,72].

4.2. Complementary Comments

The numerical simulations, corresponding to the reinforced concrete frame models K_7, K_7_S_1, K_7_S_2, and K_7_S_B_1, prove the difficulty in generating solid conclusions regarding the structural seismic response only from the analysis of the values of the lateral forces, lateral displacements, and deformations (see Figures 6–8). This, in turn, dictates the necessity to graphically observe the lateral deformation mode of each analytical model (which accurately depicts the structural seismic model).

Thus, it is possible to observe the importance of identifying and locating the main failure deformations in the weakened areas (by means of vertical drilling) for the analyzed reinforced concrete frame models K_7_S_1, K_7_S_2, and K_7_S_B_1. Arguably, this is more significant than obtaining the implicit value of said deformations.

In addition to the comments above, the following aspects regarding the lateral seismic response (local and global) of the reinforced concrete frame models employed in the current study are relevant (see Figure 5):

- A reduction in the bending stiffness of the reinforced concrete slabs transversally drilled in the corner areas was registered; thus, a partial rotation of the beams was possible, together with their deformation in the marginal zones (see Figure 5(b3),(b4),(c3),(c4));
- Active cracking was registered for an important surface in the reinforced concrete slabs (transversally drilled in the corner areas), in the long and especially in the short direction of the structure;
- The cracking length of the reinforced concrete plates (transversally drilled in the corner areas) in the long direction of the structure establishes the deformation length of the longitudinal beams, as well as the value L_{pl};
- The cracking length of the reinforced concrete slabs (transversally drilled in the corner areas) in the short direction of the structure establishes the deformation length of the transversal beams, as well as the value L_{pl}; they deform intensively, actively participating in the rotation of the longitudinal beams, forming a common body together with them;
- The beam–column frame joint actively contributes to the dissipation of the seismic energy, through intensive deformation. A conservation mechanism for the said node can be observed for the K_7_S_1, K_7_S_2, and K_7_S_B_1 reinforced concrete frame models;
- The reinforced concrete beams actively contribute to the dissipation of the seismic energy for the K_7_S_1, K_7_S_2, and K_7_S_B_1 reinforced concrete frame models.

The transversal drilling (which translates to a mechanical weakening) in the corner areas of the plates (and in the marginal zones of the beams for the K_7_S_B_1 model) significantly reduces the bending stiffness influence of the plates upon the beams, which, nevertheless, form a common body with the plates and the beam–column frame nodes;

- The RC beams will rotate as much as the RC slab will rotate;
- The reinforced concrete columns actively contribute to the dissipation of the seismic energy for all the analytical models, but there is noted conservation of their deformation degree in the end zones for the K_7_S_1, K_7_S_2, and K_7_S_B_1 models;
- The maximum considered number of transversal holes in the corner zones of the RC slabs for the K_7_S_1 analytical model leads to the deformation and maximum rotation of the beams in the marginal areas;
- The maximum considered number of transversal holes in the corner zones of the RC slabs for the K_7_S_1 analytical model leads to the deformation, cracking, and maximum rotation of the plates, both in the weakened areas and in the remaining in-between areas, favoring the occurrence of deformations and the yielding of the reinforcement bars;
- The maximum considered number of transversal holes in the corner zones of the RC slabs for the K_7_S_1 leads to the partial conservation of the beam–column frame joint, which, for all the studied situations, forms a common body with the RC slab and RC beams;
- The maximum considered number of transversal holes in the corner zones of the RC plates for the K_7_S_1 leads to the partial conservation of the marginal zones of the reinforced concrete columns, which contribute to the dissipation of the seismic energy;
- "The curves represented in Figures 6–8 prove the incapacity for a complete visualisation of the global seismic response mode of the structures and can even lead to the obtainment of wrong conclusions. Thus, by analyzing the bilinearised SPO curves from Figure 4, a conclusion that the unaffected model K_7 presents a global seismic response superior to the other analytical models may be reached" [28].

In these conditions, it is possible to observe that the seismic-resistant MR RC frame models K_7_S_1 and K_7_S_B_1 exhibit the most favourable local and global seismic response (thus, partially respecting the theoretical seismic response specifications found in P100-1 [29] and EC 8 [30] norms), in contrast with the unmodified K_7 analytical model.

The values corresponding to the forces $F^*{}_y$ and to the displacements $d^*{}_y$, which correspond to the yielding of the equivalent SDOF structural systems for K_7, K_7_S_2, K_7_S_1, and K_7_S_B_1—which can be viewed in Table 3—were determined in accordance with the requirements laid out in EC8 [30] regarding the bilinearisation process of the "F-D" capacity curves from Figure 6. The bilinearisation was performed with SPO2FRAG computer software [65,66]. The bilinearised curves are represented in Figure 4a–d.

5. Conclusions

The conclusions regarding the local and global deformation mode of the reinforced concrete frame structures analysed in the current study are synthesised in Table 5.

Table 5. General aspects (conclusions) regarding the structural degradation response of the analytical MR RC frame models.

NSC	RC Beams Cracking Process		RC Columns Cracking Process		RC Slabs Cracking Process		RC Column-Beam Joint Cracking	Final Rupture -RC Structural Element/Elements	Zone/Zones of Final Rupture	RC Beam Cracking Length Limiting by RC Slab Cracking Area	Risk of the Common Rigid Block RC "Beam-slab-Frame Node" Formation	Concrete Cracks Migration Process from the Longitudinal Beams to the Transverse Beams in the Adjacent Area of the Frame Node	GR
	Local—in Potential Plastic Zones	on Entire Length	Local—in Marginal Areas	on Entire Height	Local Area	Extended Area							
K_7	low	-	intense	low	low	medium to intense	intense	columns and nodes	marginal zones of the columns; entire volume of the nodes	yes	high with practical formation	low to insignificant	Figure 5a
K_7_S_2	low to medium	-	medium	low	low	medium	medium to intense	beams, slabs and nodes	corner area with reduced cross-section of the slabs; minor marginal zones of the beams; partial volume of the nodes	yes	medium to high with partial formation	low to medium	Figure 5b
K_7_S_1	medium	-	medium	low	medium	medium	medium to intense	beams, slabs and nodes	corner area with reduced cross-section of the slabs; minor marginal zones of the beams	yes	medium to high with partial formation	low to medium	Figure 5c
K_7_S_B_1	medium to intense	-	medium	low	medium to intense	medium to intense	medium	beams, slabs and nodes	marginal zones of the beams in reduced cross-sections; corner area for reduced cross-section of the slabs; partial volume of the beam–column joints	partial with limited influence	medium with low process formation	medium to high	Figure 5d

Note: NSC—**N**umerical **S**imulation **C**ode; RC—**R**einforced **C**oncrete; GR—**G**raphical **R**epresentation. Specified conclusions in the current table were developed based on the recorded observations at each lateral loading step for each MR RC frame model. Specified figures in the GR section (column) correspond to the seismic response of the MR RC frame systems (considered laterally loaded with equivalent static forces) in the ultimate horizontal loading step.

Furthermore, several conclusions and observations pertinent for the K_7_S_2, K_7_S_1, and K_7_S_B_1 analytical models, which were laterally loaded with equivalent static forces, can be consulted below:

- The validation of the method for improving the global seismic response and the local seismic response by means of reducing the transversal section of the reinforced concrete slabs via vertical drilling in their corner areas was accomplished;
- The guiding and concentration of the principal fracture strains (PFSM) of the concrete in the marginal (“weakened”) areas of the slabs with a reduced section (through the employment of vertically drilled holes) was achieved;
- The migration of cracks from the marginal areas of the longitudinal beams to the transversal ones along the path of the corner zones of the drilled slabs was observed; as such, a partial “conservation” of the structural integrity of the beam–column frame node was attained;
- The intense cracking of the RC slabs in the in-between areas was observed;
- The imposing length of the plastic rotation of the beams by the deformation length of the reinforced concrete slabs was noted;
- The yielding of the reinforcement located in the tensed (end) areas of the longitudinal and transversal beams was observed;
- The cracking and intense deformation of the concrete in the marginal areas of the reinforced concrete beams was noted;
- The partial development of the ”beams-slab-frame nodes” common rigid block was achieved;
- The reduction of the influence of the bending stiffness of the slabs upon the reinforced concrete beams was achieved;
- The partial development of the marginal deformation zones of the reinforced concrete columns was detected;
- The development of a complex seismic energy dissipation mechanism, in which all the structural elements contribute to the plastic deformation (but which also has positive implications regarding the reduction in the deformability of the columns at the end areas and the partial conservation of the structural integrity of the beam–column frame nodes), was achieved.

The “F-D” capacity curves corresponding to the bilinearised curves of the K_7_S_2, K_7_S_1, and K_7_S_B_1 analytical models cannot constitute a realistic image regarding the local and global seismic energy dissipation mechanisms.

Thus, there is a necessity to graphically observe and study the real deformation mode of the lateral structure. This observation is rooted in the fact that the seismic response for the K_7_S_1 and K_7_S_2 analytical models is—numerically-wise—inferior to the seismic response obtained from the K_7 model. However, from the point of view of the seismic energy dissipation mechanisms, the two models prove to be superior to the K_7 model, as real deformation concentrations can be observed in the marginal areas of the reinforced concrete beams.

In these conditions, the method of vertically drilling the corner areas of the RC slabs is validated, the efficiency of the method being observable for the analytical model with the maximum number of holes (the K_7_S_1 model). As such, it is recommended to apply this method both for new reinforced concrete frame structures, as well as for existing structures that exhibit increased vulnerability and cannot develop a global plastic mechanism in accordance with currently standing design norms.

Author Contributions: Conceptualization, I.S. and B.-I.L.; Data curation, P.M. and F.N.; Formal analysis, I.S. and F.N.; Investigation, V.N.; Methodology, P.M. and M.A.; Project administration, V.N. and M.A.; Resources, T.-C.P., V.N. and B.-I.L.; Validation, P.M. and T.-C.P.; Visualization, F.N. and B.-I.L.; Writing—original draft, I.S.; Writing—review & editing, T.-C.P. and M.A. All authors have read and agreed to the published version of the manuscript.

Funding: This research received no external funding.

Institutional Review Board Statement: Not applicable.

Informed Consent Statement: Not applicable.

Data Availability Statement: Data will be available upon request.

Conflicts of Interest: The authors declare no conflict of interest.

References

1. Mizushima, Y.; Kinoshita, T. Blind analysis on the shaking table test of a 7-story reinforced concrete building using a detailed finite element model. *J. Build. Eng.* **2022**, *52*, 104368. [CrossRef]
2. Nagender, T.; Parulekar, Y.M.; Selvam, P.; Chattopadhyay, J. Experimental study and numerical simulation of seismic behaviour of corroded reinforced concrete frames. *Structures* **2022**, *35*, 1256–1269. [CrossRef]
3. Colangelo, F. Effect of earthquake statistically correlated vertical component on inelastic demand to regular reinforced-concrete frames. *Eng. Struct.* **2020**, *211*, 110492. [CrossRef]
4. Mkrtychev, O.V.; Busalova, M.S. Calculation of reinforced concrete structures with a set seismic stability level on an earthquake. *Procedia Eng.* **2016**, *153*, 475–482. [CrossRef]
5. Socοcol, I.; Olteanu-Donțov, I.; Mihai, P.; Iftode, V.-I. Seismic response of $\frac{1}{2}$ scaled two storey reinforced concrete moment resisting frame system using nonlinear static analysis, Computational Civil Engineering (CCE 2021). *IOP Conf. Ser. Mater. Sci. Eng.* **2021**, *1141*, 012009. [CrossRef]
6. Sococol, I.; Mihai, P.; Toma, I.-O.; Venghiac, V.-M.; Olteanu-Dontov, I. Influence of Concrete Strength Class on the Plastic Hinges Location for a Reinforced Concrete Moment-Resisting Frame Structure with Consideration of the Horizontal Stiffening Effect of the Slab. *Bull. Polytech. Inst. Jassy Constr. Archit. Sect.* **2020**, *66*, 95–108.
7. Sococol, I.; Mihai, P.; Toma, I.-O.; Venghiac, V.-M.; Olteanu-Dontov, I. Static Non-linear Analysis of an RC Moment Resisting Frame by Considering Different Values for the Longitudinal Reinforcement Ratio in the Columns. *Bull. Polytech. Inst. Jassy Constr. Archit. Sect.* **2020**, *66*, 91–106.
8. Sococol, I.; Mihai, P.; Toma, I.-O.; Olteanu-Dontov, I.; Venghiac, V.-M. The Influence of the RC Beams Cross Section on the Dissipative Seismic Response of a Moment Resisting RC Frame System. *Bull. Polytech. Inst. Jassy Constr. Archit. Sect.* **2020**, *66*, 21–38.
9. Sococol, I.; Petrescu, T.C.; Mihai, P.; Babor, D.T. Influence of the longitudinal steel ration in RC beams and steel reinforcement ration in RC slabs on the seismic energy dissipation mechanisms for a MR RC frame structure, Civil Engineering Conference (CEC 2022). *IOP Conf. Ser. Mater. Sci. Eng.* **2022**. *Unpublished results-pending publication*.
10. Baloevic, G.; Radnic, J.; Grgic, N.; Grubisic, I. Shake-table study on the effect of masonry infill on the seismic response of reinforced concrete frames. *Soil Dyn. Earthq. Eng.* **2022**, *161*, 107404. [CrossRef]
11. *Engineering Aspects of the 1971 San Fernando Earthquake*; Building Science Series 40; U.S. Department of Commerce: Washington, DC, USA, 1971.
12. *An Investigation of the Miyagi-ken-oki, Japan, Earthquake of June 12, 1978*; NBS Special Publication 592; U.S. Department of Commerce: Washington, DC, USA, 1980.
13. *The Imperial Valley, California, Earthquake of October 15, 1979*; Geological Survey Professional Paper 1254; U.S. Government Printing Office: Washington, DC, USA,, 1982.
14. *1994 Northridge Earthquake, Performance of Structures, Lifelines, and Fire Protection Systems*; NIST Special Publication 862; U.S. Department of Commerce Technology Administration: Washington, DC, USA, 1994.
15. *The January 17, 1995 Hyogoken-Nanbu (Kobe) Earthquake*; NIST Special Publication 901; U.S. Government Printing Office: Washington, DC, USA, 1996.
16. *The Aegean Earthquake and Tsunami of 30 October 2020*; A Field Report; EEFIT (Earthquake Engineering Field Investigation Team): London, UK, 2021.
17. Liu, Y.; Zhao, Z.; Cheng, X.; Li, Y.; Diao, M.; Sun, H. Experimental and numerical investigation of the progressive collapse of precast reinforced concrete frame substructures with wet connections. *Eng. Struct.* **2022**, *256*, 114010. [CrossRef]
18. Kokot, S. Response spectrum of a reinforced concrete frame structure under various column removal scenarios. *J. Build. Eng.* **2022**, *49*, 103992. [CrossRef]
19. Yu, D.-H.; Li, G.; Dong, Z.-Q.; Li, H.-N. A fast and accurate method for the seismic response analysis of reinforced concrete frame structures considering Beam-Column joint deformation. *Eng. Struct.* **2022**, *251*, 113401. [CrossRef]
20. Perceka, W.; Djayaprabha, H.S.; Laurensia, C.; Wirawan, R.M. Seismic performance evaluation for 20-story RC special moment frame structure made of highly flowable-strain hardening fiber reinforced concrete (HF-SHFRC). *Mater. Today Proc.* **2022**, *65*, 983–987. [CrossRef]
21. Rajeev, A.; Parsi, S.S.; Raman, S.N.; Ngo, T.; Shelke, A. Experimental and numerical investigation of an exterior reinforced concrete beam-column joint subjected to shock loading. *Int. J. Impact Eng.* **2020**, *137*, 103473. [CrossRef]
22. Jiang, P.; Zheng, H.; Xiong, J.; Wen, P. Nonlinear elastic-plastic analysis of reinforced concrete column-steel beam connection by RBF-FD method. *Eng. Anal. Bound. Elem.* **2021**, *128*, 188–194. [CrossRef]

23. Alavi-Dehkordi, S.; Mostofinejad, D.; Alaee, P. Effects of high-strength reinforcing bars and concrete on seismic behavior of RC beam-column joints. *Eng. Struct.* **2019**, *183*, 702–719. [CrossRef]
24. Karthik, M.M.; Mander, J.B.; Hurlebaus, S. Simulating behaviour of large reinforced concrete beam-column joints subject to ASR/DEF deterioration and influence of corrosion. *Eng. Struct.* **2020**, *222*, 111064. [CrossRef]
25. Allam, S.M.; Elbakry, H.M.F.; Arab, I.S.E. Exterior reinforced concrete beam column joint subjected to monotonic loading. *Alex. Eng. J.* **2018**, *57*, 4133–4144. [CrossRef]
26. Zhang, J.; Pei, Z.; Rong, X. Experimental seismic study of an innovative precast steel-concrete composite beam-column joint. *Soil Dyn. Earthq. Eng.* **2022**, *161*, 107420. [CrossRef]
27. Zhang, Y.; Li, B.; Li, Z.; Ma, G.; Liu, Y. Seismic performance of interior beam-column joints in reinforced glazed hollow bead insulation concrete frames. *Eng. Struct.* **2021**, *228*, 111494. [CrossRef]
28. Sococol, I.; Mihai, P.; Petrescu, T.-C.; Nedeff, F.; Nedeff, V.; Agop, M. Analytical Study Regarding the Seismic Response of a Moment-Resisting (MR) Reinforced Concrete (RC) Frame System with Reduced Cross Sections of the RC Beams. *Buildings* **2020**, *12*, 983. [CrossRef]
29. *Cod de proiectare seismică", Partea I, Prevederi de proiectare pentru clădiri, Indicativ P100-1*; Ministerul Dezvoltării Regionale și Administrației Publice, UTCB: București, Romania, 2013.
30. *Eurocod 8: Proiectarea structurilor pentru rezistența la cutremur, Partea 1: Reguli generale, acțiuni seismice și reguli pentru clădiri, Indicativ SR EN 1998-1*; ASRO: București, Romania, 2004. (In Romanian)
31. ATENA Software. Available online: https://www.cervenka.cz (accessed on 17 January 2021).
32. Mihai, P.; Hirhui, I.; Rosca, B. Numerical Analysis of Bonding Between Concrete and Reinforcement using the Finite Element Method. *J. Appl. Sci.* **2010**, *10*, 738–744. [CrossRef]
33. Siempu, R.; Pancharathi, R.K. Numerical study on the bond behaviour of plain and ribbed bars in self-compacting concrete. *Mater. Today Proc.* **2022**, *51*, 2587–2591. [CrossRef]
34. Don, W.; Suryanto, B.; Tambusay, A.; Suprobo, P. Forensic assessments of the influence of reinforcement detailing in reinforced concrete half-joints: A nonlinear finite element study. *Structures* **2022**, *38*, 689–703. [CrossRef]
35. Paz, G.L.G.; Marques, M.G.; Ruas, S.R.C. Numerical analysis of reinforced concrete columns strengthened with sleeve wedge bolts and a self compacting concrete layer. *Structures* **2022**, *43*, 726–737. [CrossRef]
36. Kannam, P.; Sarella, V.R. A study on validation of shear behaviour of steel fibrous SCC based on numerical modelling (ATENA). *J. Build. Eng.* **2018**, *19*, 69–79. [CrossRef]
37. Hoang, A.L.; Fehling, E. Numerical study of circular steel tube confined concrete (STCC) stub columns. *J. Constr. Steel Res.* **2017**, *136*, 238–255. [CrossRef]
38. Safdar, M.; Sheikh, M.N.; Hadi, M.N.S. Numerical study on shear strength of GFRP-RC T-Joints. *Structures* **2022**, *43*, 926–943. [CrossRef]
39. Sanabria Diaz, R.A.; Sarmiento Nova, S.J.; Teixeira da Silva, M.C.A.; Trautwein, L.M.; Almeida, L.C. Reliability analysis of shear strength of reinforced concrete deep beams using NLFEA. *Eng. Struct.* **2020**, *203*, 109760. [CrossRef]
40. Faria, R.; Marreiros, R.; Ramos, A.P.; Jesus, C. Influence of the top reinforcement detailing in the behaviour of flat slabs. *Structures* **2020**, *23*, 718–730. [CrossRef]
41. Mousavi, S.S.; Dehestani, M. Influence of mixture composition on the structural behaviour of reinforced concrete beam-column joints: A review. *Structures* **2022**, *42*, 29–52. [CrossRef]
42. Men, J.; Xiong, L.; Wang, J.; Fan, G. Effect of different RC slab widths on the behavior of reinforced concrete column and steel beam-slab subassemblies. *Eng. Struct.* **2021**, *229*, 111639. [CrossRef]
43. Chu, L.; Tian, Y.; Li, D.; He, Y.; Feng, H. Shear behavior of steel reinforced concrete column-steel beam joints with or without reinforced concrete slab. *J. Build. Eng.* **2021**, *35*, 102063. [CrossRef]
44. El-Attar, A.G.; White, R.N.; Gergely, P. *Shake Table Test of a 1/6 Scale Two-Story Lightly Reinforced Concrete Building*; Cornell University: New York, NY, USA, 1991.
45. Harris, H.G.; Sabnis, G.M. *Structural Modeling and Experimental Techniques*, 2nd ed.; CRC Press: Boca Raton, FA, USA, 1999.
46. Moncarz, P.D.; Krawinkler, H. *Theory and Application of Experimental Model Analysis in Earthquake Engineering*; Stanford University: San Jose, FA, USA, 1981.
47. Zwart, S.D. Scale Modelling in Engineering: Froude's Case. In *Handbook of the Philosophy of Science*; Elsevier: Amsterdam, The Netherlands, 2009; pp. 759–798. [CrossRef]
48. Kenan, H.; Azeloglu, O. Design of scaled down model of a tower crane mast by using silimitude theory. *Eng. Struct.* **2020**, *220*, 110985. [CrossRef]
49. Wang, Z.; Li, S.; Lu, S.; Yu, S. Model investigations for seismic responses of a scaled polar crane at a nuclear power station. *Nucl. Eng. Des.* **2021**, *381*, 111330. [CrossRef]
50. Yazdandoust, M.; Samee, A.A.; Ghalandarzadeh, A. Assessment of seismic behavior of back-to-back mechanically stabilized earth walls using 1g shaking table tests. *Soil Dyn. Earthq. Eng.* **2022**, *155*, 106078. [CrossRef]
51. Richard, B.; Ile, N.; Frau, A.; Ma, A.; Loiseau, O.; Giry, C.; Ragueneau, F. Experimental and numerical study of a half-scaled reinforced concrete building equipped with thermal break components subjected to seismic loading up to severe damage state. *Eng. Struct.* **2015**, *92*, 29–45. [CrossRef]

52. Richard, B.; Martinelli, P.; Voldoire, F.; Corus, M.; Chaudat, T.; Abouri, S.; Bonfils, N. SMART 2008: Shaking table tests on an asymmetrical reinforced concrete structure and seismic margins assessment. *Eng. Struct.* **2015**, *105*, 48–61. [CrossRef]
53. Bitencourt, L.A.G., Jr.; Manzoli, O.L.; Trindade, Y.T.; Rodrigues, E.A.; Dias-da-Costa, D. Modeling reinforced concrete structures using coupling finite elements for discrete representation of reinforcements. *Finite Elem. Anal. Des.* **2018**, *149*, 32–44. [CrossRef]
54. Sousa, J.B.M., Jr.; Muniz, C.F.D.G. Analytical integration of cross section properties for numerical analysis of reinforced concrete, steel and composite frames. *Eng. Struct.* **2007**, *29*, 618–625. [CrossRef]
55. Sococol, I.; Mihai, P.; Toma, I.-O.; Olteanu-Dontov, I.; Venghiac, V.-M. Stress-Strain Relation Laws for Concrete and Steel Reinforcement Used in Non-linear Static Analytical Studies of the Moment Resisting Reinforced Concrete (RC) Frame Models. *Bull. Polytech. Inst. Jassy Constr. Archit. Sect.* **2021**, *67*, 17–29. [CrossRef]
56. Shiming, S.; Yupu, S. Dynamic biaxial tensile-compressive strength and failure criterion of plain concrete. *Constr. Build. Mater.* **2013**, *40*, 322–329. [CrossRef]
57. Ivashenko, Y.; Ferder, A. Experimental studies on the impacts of strain and loading modes on the formation of concrete "stress-strain" relations. *Constr. Build. Mater.* **2019**, *209*, 234–239. [CrossRef]
58. Bi, J.; Huo, L.; Zhao, Y.; Qiao, H. Modified the smeared crack constitutive model of fiber reinforced concrete under uniaxial loading. *Constr. Build. Mater.* **2020**, *250*, 118916. [CrossRef]
59. Wei, H.; Wu, T.; Liu, X.; Zhang, R. Investigation of stress-strain relationship for confined lightweight aggregate concrete. *Constr. Build. Mater.* **2020**, *256*, 119432. [CrossRef]
60. Dong, S.; Wang, Y.; Ashour, A.; Han, B.; Ou, J. Uniaxial compressive fatigue behavior of ultra-high performance concrete reinforced with super-fine stainless wires. *Int. J. Fatigue* **2021**, *142*, 105959. [CrossRef]
61. Xu, T.; Castel, A.; Gilbert, R.I.; Murray, A. Modeling the tensile steel reinforcement strain in RC-beams subjected to cycles of loading and unloading. *Eng. Struct.* **2016**, *126*, 92–105. [CrossRef]
62. Wang, Z.-H.; Li, L.; Zhang, Y.-X.; Zheng, S.-S. Reinforcement model considering slip effect. *Eng. Struct.* **2019**, *198*, 109493. [CrossRef]
63. Long, X.; Wang, C.-Y.; Zhao, P.-Z.; Kang, S.-B. Bond strength of steel reinforcement under different loading rates. *Constr. Build. Mater.* **2020**, *238*, 117749. [CrossRef]
64. Sabău, M. Simulated data on bond of steel reinforcement in self-compacting concrete. *Data Brief* **2020**, *30*, 105594. [CrossRef] [PubMed]
65. Baltzopoulos, G.; Baraschino, R.; Iervolino, I.; Vamvatsikos, D. SPO2FRAG: Software for seismic fragility assessment based on static pushover. *Bull Earthq. Eng.* **2017**, *15*, 4399–4425. [CrossRef]
66. Baltzopoulos, G.; Baraschino, R.; Iervolino, I.; Vamvatsikos, D. *SPO2FRAG [Computer Software]*; AXA-DiSt (Universita degli Studi di Napoli Federico II): Naples, Italy, 2017.
67. *Eurocod 8: Proiectarea Structurilor pentru Rezistența la Cutremur, Partea 1: Reguli Generale, Acțiuni Seismice și Reguli Pentru Clădiri, Anexa Națională, Indicativ SR EN 1998-1*; ASRO: București, Romania, 2008. (In Romanian)
68. Paulay, T.; Priestley, M.J.N. *Seismic Design of Reinforced Concrete and Masonry Buildings*; John Wiley & Sons: Hoboken, NJ, USA, 1992.
69. Anas, S.M.; Alam, M.; Shariq, M. Damage Response of Conventionally Reinforced Two-Way Spanning Concrete Slab under Eccentric Impacting Drop Weight Loading. In *Defence Technology*; Elsevier: Amsterdam, The Netherlands, 2022; ISSN 2214–9147. [CrossRef]
70. Anas, S.M.; Shariq, M.; Alam, M. Evaluation of critical damage location of contact blast on conventionally reinforced one-way square concrete slab applying CEL-FEM blast modelling technique. *Int. J. Prot. Struct.* **2022**. [CrossRef]
71. Anas, S.M.; Alam, M.; Umair, M. Experimental and numerical investigations on performance of reinforced concrete slabs under explosive-induced air-blast loading: A state-of-the-art review. *Structures* **2021**, *31*, 428–461. [CrossRef]
72. *Eurocod 2: Proiectarea structurilor de beton, Partea 1-1: Reguli generale și reguli pentru clădiri, Indicativ SR EN 1992-1-1*; ASRO: București, Romania, 2006. (In Romanian)